Preprint to a paper submitted to *Ship Technology Research/Schiffstechnik* and later published at
https://www.tandfonline.com/10.1080/09377255.2021.1966575 in 2021.

A Comprehensive and Practical Guide to the Hess and Smith Constant Source and Dipole Panel

Lothar Birk

School of Naval Architecture and Marine Engineering
2000 Lakeshore Drive, New Orleans, LA 70148, USA, E-mail: lbirk@uno.edu

Abstract

In a series of landmark reports and papers J.L. Hess and A.M.O. Smith introduced the quadrilateral constant source panel to solve three-dimensional nonlifting potential flow problems (Hess and Smith, 1962, 1964, 1967). Later a panel with constant dipole (doublet) distribution was added for lifting flow computations (Hess, 1972). The cited publications provide equations for the computation of the velocities induced by the singularity distributions along with required geometric properties of the panel. Equations are presented considering an implementation in Fortran (Versions II and IV), the commonly used programming language for numerical methods at the time. The present paper builds on Hess & Smith's groundbreaking work, restating equations with modern programming languages in mind capable of fast vector operations like Fortran 95, Python or Julia. Formulas are provided for the computation of geometric properties, coordinate transformations, as well as first and second order potential derivatives. Example input and output data allow readers to test and validate their own implementation.

Keywords: potential flow, panel method, Rankine panel, dipole panel

1 Introduction

Computational Fluid Dynamics (CFD) plays an important role in the design of aircraft, ships and their propulsion systems. High fidelity CFD tools solve the Reynolds Average Navier-Stokes Equations (RANSE) for incompressible and compressible viscous fluids. However, despite all the advances in accuracy and stability of algorithms and the growth in computational power in recent years, computation times for RANSE solvers are still high and often render their use impractical in early design phases.

In quite a number of practical applications viscosity of the fluid may be neglected which simplifies mathematical modeling and numerical solutions. Assuming the fluid can be treated as inviscid, incompressible and irrotational in simply connected regions the continuity equation may be replaced by the Laplace equation. Combined with appropriate boundary conditions the Laplace equation yields a velocity potential ϕ (Kellogg, 1929). The velocity field $\underline{v}_g$ [1] is given by the gradient of the potential:

$$\underline{v}_g = \underline{\nabla}_g \Phi = \begin{pmatrix} \frac{\partial \Phi}{\partial x} \\ \frac{\partial \Phi}{\partial y} \\ \frac{\partial \Phi}{\partial z} \end{pmatrix} = \begin{pmatrix} u_g \\ v_g \\ w_g \end{pmatrix} \tag{1}$$

Especially effective in the solution of potential flow problems are panel methods which fall into the general category of boundary element methods. Any potential flow may be represented by a combined distribution of sources and dipoles over the boundaries of the flow domain. This is a well documented foundation of

[1] In this paper vector quantities are indicated by underlining, e.g. $\underline{v}$ for the velocity vector. Matrices are indicated by double underlining.

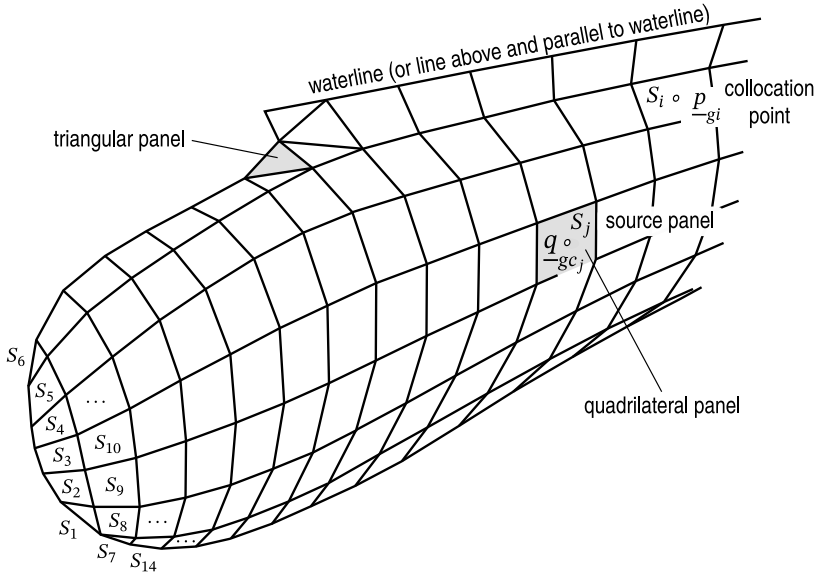

Figure 1: Discretization of a ship bow into quadrilateral and triangular panels (Birk, 2019)

potential flow theory. A summary is shown for instance in Katz and Plotkin (2001). The big advantage of this method is that the dimension of the problem is reduced from a three-dimensional volume to a two-dimensional surface. Therefore, only the limiting surfaces of the fluid domain need to be disctretized instead of the three-dimensional fluid domain resulting in a substantial reduction of the numerical grid size and computation time. To list just a few of its many applications, panel methods are used in the computation of lifting flows around aircraft (Hess, 1972; J.L. and W.O., 1988), propellers (Hsin et al., 1991; Kinnas et al., 2015), and cavitating flows (Mishima and Kinnas, 1997; Gaggero and Brizzolara, 2009), as well as nonlifting flows for ship wave resistance computations (Dawson, 1977; Jensen, 1988; Raven, 1996; Janson, 1997; Bal, 2008), seakeeping problems (Newman and Sclavounos, 1988; Nakos, 1990; Lee et al., 1996; Kim and Shin, 2003), and associated hull shape optimization procedures (Harries, 1998; Grigoropoulos et al., 2003; Birk, 2009).

In panel methods the actual body surface is subdivided into small triangular or quadrilateral patches known as panels S_j (Figure 1). Each panel features surface distributions of Rankine sources ϕ_r of strength σ and possibly normal dipoles ϕ_d of strength μ. Here the following definitions are used:

$$\text{Rankine source}: \quad \phi = \sigma\left(\frac{-1}{4\pi r}\right) \qquad \text{Normal dipole (doublet)}: \quad \psi = -\mu\,\frac{\partial}{\partial n}\left(\frac{-1}{4\pi r}\right) \tag{2}$$

The dipole distribution is necessary if lifting flows are modeled. The distance r is measured between a field point $\underline{p}_g = (x_g, y_g, z_g)^T$ and a source or dipole point $\underline{q}_g = (\xi_g, \eta_g, \zeta_g)^T$.

$$r = \sqrt{(x_g - \xi_g)^2 + (y_g - \eta_g)^2 + (z_g - \zeta_g)^2} \tag{3}$$

Integration of the source and dipole distributions yields the contribution of a panel to the overall potential.

$$\Phi_j = \iint_{S_j} \phi \,\mathrm{d}S + \iint_{S_j} \psi \,\mathrm{d}S \tag{4}$$

In order to extract the unknown source and dipole strengths from the integrals, assumptions are made about the shape of the distributions. Most commonly, source and dipole strength are assumed to be constant on each panel. This approach is discussed in the present paper. However, linear and higher order distributions are also in use, see for example (Maniar, 1995; Katz and Plotkin, 2001).

As mentioned in the summary, J.L. Hess and A.M.O. Smith introduced the quadrilateral constant source panel to solve three-dimensional nonlifting potential flow problems (Hess and Smith, 1962, 1964, 1967). A panel

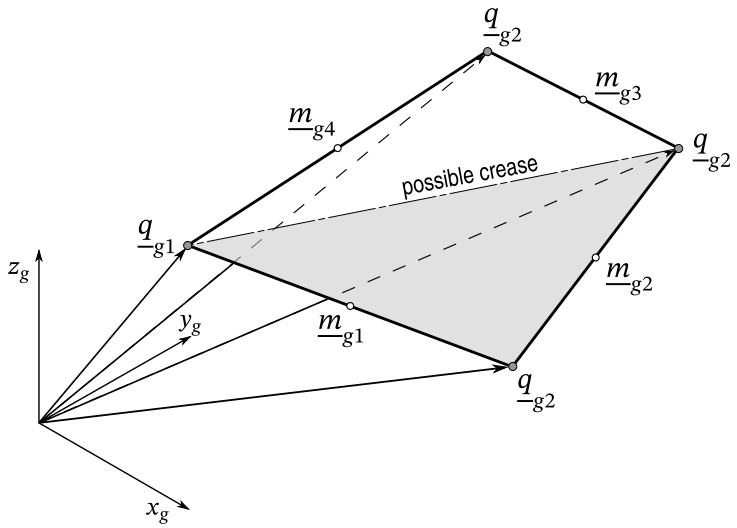

Figure 2: Quadrilateral panel in the global coordinate system $< x_g, y_g, z_g >$

with constant dipole distributions was added later for lifting flows (Hess, 1972). This topic was later revisited by R. Yeung and W.C. Webster for triangular panels (Yeung, 1973; Webster, 1975). In another important publication, Newman (1986) presented a unified derivation of the potential of quadrilateral and triangular panels with constant and higher order distributions of source and normal dipoles.

The idea for the present paper arose from a graduate course in which the students implement a panel method for the calculation of wave resistance. Combing through the original publications proofed time consuming and error prone because of differences in notation and definitions. For instance, in older literature velocity $\underline{v}$ was defined as the negative gradient of the potential whereas nowadays the definition $\underline{v} = +\underline{\nabla}\phi$ is more common. In addition, equations for the second order derivatives of the potential are hard to find. Hence this summary was written, and although the present paper does not expand the theory for quadrilateral source and dipole panels, it comes in handy for researchers who wish to implement their own panel method. A set of sample data enables testing and validation of the implementation.

Section 2 below presents the derivation and formulas for geometric properties of a panel which are used in subsequent computations. Section 3 discusses the transformations of vectors from a global to a local panel coordinate system and explains how results obtained in the local panel coordinate system are transferred back into the global coordinate system. The fourth Section states the formulas for the computation of first and second order derivatives of the potential induced by a panel with a constant strength source distribution. Section 5 provides the equivalent formulas for a panel with a constant strength normal dipole distribution. Section 6 briefly touches on approximating the effects of a panel by a single point source or dipole. These can be used to shorten computation time if the field point is far enough away from the panel. In Section 7 input data and results are presented for three test panels. Conclusions wrap up the paper.

2 Panel geometry

The geometry of the body or hull is usually described in a body-fixed coordinate system $< x_g, y_g, z_g >$. Each quadrilateral panel is defined by a set of four corner points $\underline{q}_{g1}g'$, $\underline{q}_{g2}$, $\underline{q}_{g3}$, and $\underline{q}_{g4}$ (Figure 2). Potential and velocity induced by a panel at a given field point $\underline{p}_g$ are evaluated in a panel-specific local Cartesian coordinate system $< x, y, z >$. The local x and y directions span the tangent plane of the panel and the positive z-axis points into the direction of panel surface normal vector $\underline{n}_g$. Triangular panels are obtained when two adjacent points coincide. The latter works best if first and last point are made identical.

Besides the unit vectors $\underline{s}_g$, $\underline{t}_g$, and $\underline{n}_g$ for the local coordinate system $< x, y, z >$, we also need to determine panel corners in local coordinates, as well as area A, and centroid q_{gc} of the panel. Higher order moments of

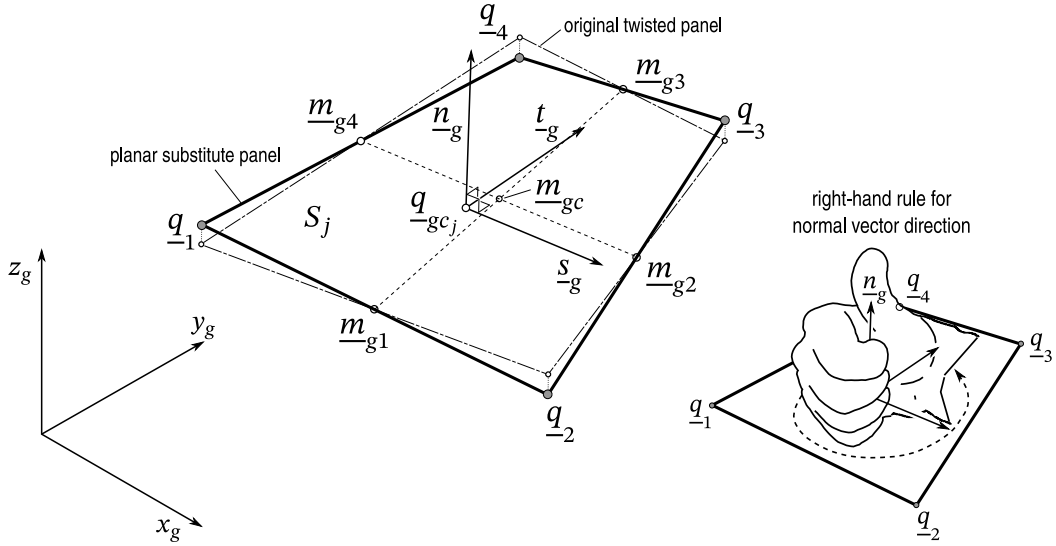

Figure 3: Planar quadrilateral panel with local coordinate system

the panel area are needed in cases where multi-pole expansions are employed to speed up the computation of influence coefficients. In the following sections, we derive the needed geometric properties of the panel from its given corner point coordinates.

2.1 Local coordinate system

One of the drawbacks of quadrilateral panels is that they are not necessarily flat. As indicated in Figure 2 by the shading of the panel surface, a crease might exist along one of its diagonals. It is common practice for constant source and dipole panels to replace the original panel with a planar equivalent. This might cause small gaps between adjacent panels. If the gaps become intolerably wide, twisted quadrilaterals should be split into triangular panels. Despite this drawback quadrilateral panels are preferred because they reduce the number of panels which is a driving factor for computation time.

A quadrilateral is planar, if its diagonals intersect in a common point. Although the diagonals of the panel from $\underline{q}_{g1}$ to $\underline{q}_{g3}$ and $\underline{q}_{2g}$ to $\underline{q}_{g4}$ may not always intersect, the lines connecting the midpoints of the panel edges $\underline{m}_{gk}$ with $k = 1, 2, 3, 4$ always do (Figures 2 and 3). These lines are known as bimedians. The midpoints of panel edges are obtained by averaging two adjacent corner points.

$$\underline{m}_{gk} = \frac{1}{2}\left(\underline{q}_{gk} + \underline{q}_{g,k+1}\right) \qquad \text{with } k \in \{1,2,3,4\} \text{ and } k+1 \in \{2,3,4,1\} \tag{5}$$

Note that we use a cyclic index for the panel corners, i.e. given an edge or corner point index k the subsequent index is defined as $k{+}1 := \mathrm{mod}(k,4){+}1$. The modulus function $\mathrm{mod}(k,4)$ yields the remainder of the integer division $k/4$ (e.g. $\mathrm{mod}(3,4) = 3$, $\mathrm{mod}(4,4) = 0$).

The midpoint of the first bimedian from $\underline{m}_{g1}$ to $\underline{m}_{g3}$ is identical to the midpoint of the second bimedian from $\underline{m}_{g4}$ to $\underline{m}_{g2}$. The intersection point $\underline{m}_{gc}$ is known as vertex centroid.

$$\underline{m}_{gc} = \frac{1}{2}\left(\underline{m}_{g1} + \underline{m}_{g3}\right) = \frac{1}{2}\left(\underline{m}_{g2} + \underline{m}_{g4}\right) = \frac{1}{4}\left(\underline{q}_{g1} + \underline{q}_{g2} + \underline{q}_{g3} + \underline{q}_{g4}\right) \tag{6}$$

Thus $\underline{m}_{g1}$ through $\underline{m}_{g4}$ define a plane which we will use to define a planar panel substituting for $\underline{q}_{g1}$ through $\underline{q}_{g4}$. Note that vertex centroid and area centroid typically mark different points.

The corner point sequence determines the direction of the panel normal vector $\underline{n}_g$ based on a right-hand rule as shown in Figure 3.

We select the direction of the local x-coordinate to coincide with the direction given by the vector pointing from $\underline{m}_{g4}$ to $\underline{m}_{g2}$:

$$\underline{s}_g = \frac{\underline{m}_{g2} - \underline{m}_{g4}}{\|\underline{m}_{g2} - \underline{m}_{g4}\|} \tag{7}$$

As a temporary second base vector for the panel plane we select the vector pointing from $\underline{m}_{g1}$ to $\underline{m}_{g3}$:

$$\bar{\underline{t}}_g = \underline{m}_{g3} - \underline{m}_{g1} \tag{8}$$

The vector $\bar{\underline{t}}_g$ is not necessarily perpendicular to $\underline{s}_g$ and will be replaced shortly. Therefore, we skip normalizing it to unit length.

With the panel plane defined we are able to compute the panel normal vector:

$$\underline{n}_g = \frac{\underline{s}_g \times \bar{\underline{t}}_g}{\|\underline{s}_g \times \bar{\underline{t}}_g\|} \tag{9}$$

To complete the local coordinate system we replace $\bar{\underline{t}}'$ with

$$\underline{t}_g = \frac{\underline{n}_g \times \underline{s}_g}{\|\underline{n}_g \times \underline{s}_g\|} \tag{10}$$

This vector is obviously perpendicular to $\underline{n}_g$ and therefore lies in the panel plane.

For practical purposes we assemble the coordinates into a [3×3] transformation matrix $\underline{\underline{T}}$ each vector forming a column of the matrix.

$$\underline{\underline{T}} = \left[\underline{s}_g \;\; \underline{t}_g \;\; \underline{n}_g\right] = \begin{bmatrix} s_{gx} & t_{gx} & n_{gx} \\ s_{gy} & t_{gy} & n_{gy} \\ s_{gz} & t_{gz} & n_{gz} \end{bmatrix} \tag{11}$$

The individual vector coordinates like s_{gx}, s_{gy}, s_{gz} represent the directional cosines of the local panel axes with the global coordinate system $< x_g, y_g, z_g >$.

2.2 Temporary panel corners

We use the midpoint $\underline{m}_{gc}$ as a temporary origin to compute the coordinates of the panel corners with respect to the local coordinate system. Later we will shift the origin to the true centroid $\underline{q}_{gc}$ of the panel area.

All points on the flattened panel lie in the x-y-plane and have $z = 0$ as a third coordinate. Therefore, we will only save the local x_k, y_k-coordinates for each corner. The temporary local coordinates follow from projections of the vectors pointing from the temporary center $\underline{m}_{gc}$ to each corner $\underline{q}_{gk}$ onto the directions $\underline{s}_g$ and $\underline{t}_g$.

$$\bar{\underline{q}}_k = \begin{pmatrix} \bar{x}_k \\ \bar{y}_k \end{pmatrix} = \begin{pmatrix} \left(\underline{q}_{gk} - \underline{m}_{gc}\right)^T \underline{s}_g \\ \left(\underline{q}_{gk} - \underline{m}_{gc}\right)^T \underline{t}_g \end{pmatrix} \qquad \text{for } k = 1, 2, 3, 4 \tag{12}$$

2.3 Panel area and centroid

The area A of a panel S_j is defined as

$$A = \iint_{S_j} 1 \, \mathrm{d}x\mathrm{d}y \tag{13}$$

The first order moments with respect to x- and y-axis, M_x and M_y, are given by

$$M_x = \iint_{S_j} y \,\mathrm{d}x\mathrm{d}y \tag{14}$$

$$M_y = \iint_{S_j} x \,\mathrm{d}x\mathrm{d}y \tag{15}$$

The surface integrals in Equations (13) through (15) may be replaced by line integrals via Stokes' integral theorem.

$$\iint_S \left(\frac{\partial Q}{\partial x} - \frac{\partial P}{\partial y}\right) \mathrm{d}x\mathrm{d}y = \oint_C P \,\mathrm{d}x + \oint_C Q \,\mathrm{d}y \tag{16}$$

For instance, choosing the functions $P \equiv 0$ and $Q \equiv x$ and substituting them into Stokes' theorem (16) yields an equation for the panel area A:

$$\begin{aligned} \iint_S \left(\frac{\partial x}{\partial x} - \frac{\partial 0}{\partial y}\right) \mathrm{d}x\mathrm{d}y &= \oint_C 0 \,\mathrm{d}x + \oint_C x \,\mathrm{d}y \\ \iint_{S_j} 1 \,\mathrm{d}x\mathrm{d}y &= \oint_C x \,\mathrm{d}y \\ A &= \oint_C x \,\mathrm{d}y \end{aligned} \tag{17}$$

Selecting $P \equiv -\frac{y^2}{2} \;\wedge\; Q \equiv 0$ and $P \equiv 0 \;\wedge\; Q \equiv \frac{x^2}{2}$ yields formulae for M_x and M_y respectively.

$$M_x = \oint_C \frac{x^2}{2} \,\mathrm{d}y \tag{18}$$

$$M_y = -\oint_C \frac{y^2}{2} \,\mathrm{d}x \tag{19}$$

Our panels have straight edges which renders the solution of the line integrals straight forward. The coordinates along an edge k are expressed as linear functions of a parameter t taking values from zero to one. For $t = 0$ we are at the start point of the edge $\underline{\bar{q}}_k$, and for $t = 1$ we reach its end point $\underline{\bar{q}}_{k+1}$.

$$\begin{aligned} \underline{\bar{q}} &= (\underline{\bar{q}}_{k+1} - \underline{\bar{q}}_k)t + \underline{\bar{q}}_k \\ \begin{pmatrix} \bar{x} \\ \bar{y} \end{pmatrix} &= \begin{pmatrix} (\bar{x}_{k+1} - \bar{x}_k)t + \bar{x}_k \\ (\bar{y}_{k+1} - \bar{y}_k)t + \bar{y}_k \end{pmatrix} \end{aligned} \tag{20}$$

First, we split the line integrals into four parts, one for each edge.

$$A = \oint_C \bar{x} \,\mathrm{d}\bar{y} = \sum_{k=1}^{4} \int_{\bar{y}_k}^{\bar{y}_{k+1}} \bar{x} \,\mathrm{d}\bar{y} \tag{21}$$

Second, we substitute the integrand x with the parametric form from Equation (20).

$$A = \sum_{k=1}^{4} \int_{\bar{y}_k}^{\bar{y}_{k+1}} (\bar{x}_{k+1} - \bar{x}_k)t + \bar{x}_k \,\mathrm{d}\bar{y} \tag{22}$$

Next, we substitute the parameter t for the integration variable y.

$$\frac{\mathrm{d}\bar{y}}{\mathrm{d}t} \;=\; (\bar{y}_{k+1} - \bar{y}_k) \qquad \text{or} \qquad \mathrm{d}\bar{y} \;=\; (\bar{y}_{k+1} - \bar{y}_k)\,\mathrm{d}t$$

Variable substitution requires a change in integration limits:

$$\begin{aligned} &\text{lower limit} \quad \bar{y} = \bar{y}_k \;\longrightarrow\; t = 0 \\ &\text{upper limit} \quad \bar{y} = \bar{y}_{k+1} \longrightarrow\; t = 1 \end{aligned}$$

The equation for the panel area A now reads

$$A \;=\; \sum_{k=1}^{4} \int_0^1 \Big[(\bar{x}_{k+1} - \bar{x}_k)t + \bar{x}_k\Big](\bar{y}_{k+1} - \bar{y}_k)\,\mathrm{d}t \tag{23}$$

Finally, solving the individual integrals and simplifying the algebraic equation yields

$$A \;=\; \frac{1}{2}\sum_{k=1}^{4} (\bar{y}_{k+1} - \bar{y}_k)(\bar{x}_k + \bar{x}_{k+1}) \tag{24}$$

Choosing different functions P and Q and following the same solution process results in algebraic formulae for first order moments and, if needed, for higher order moments as well.

$$P \equiv -\frac{y^2}{2} \;\wedge\; Q \equiv 0: \qquad M_x \;=\; \iint_A y\,\mathrm{d}x\,\mathrm{d}y \;=\; -\oint_C \frac{y^2}{2}\,\mathrm{d}x$$

$$= -\frac{1}{6}\sum_{k=1}^{4} (\bar{x}_{k+1} - \bar{x}_k)(\bar{y}_k^2 + \bar{y}_k\bar{y}_{k+1} + \bar{y}_{k+1}^2) \tag{25}$$

$$P \equiv 0 \;\wedge\; Q \equiv \frac{x^2}{2}: \qquad M_y \;=\; \iint_A x\,\mathrm{d}x\,\mathrm{d}y \;=\; \oint_C \frac{x^2}{2}\,\mathrm{d}y$$

$$= \frac{1}{6}\sum_{k=1}^{4} (\bar{y}_{k+1} - \bar{y}_k)(\bar{x}_k^2 + \bar{x}_k\bar{x}_{k+1} + \bar{x}_{k+1}^2) \tag{26}$$

From the first order moments follow the coordinates of the actual centroid with respect to the temporary origin $\underline{m}_{gc}$

$$\bar{x}_c \;=\; \frac{M_y}{A} \tag{27}$$

$$\bar{y}_c \;=\; \frac{M_x}{A} \tag{28}$$

We shift the origin from $\underline{m}_{gc}$ to the true centroid location $\underline{q}_{gc}$ in global coordinates by moving a distance $\bar{x}_c$ in $\underline{s}_g$ direction and $\bar{y}_c$ in $\underline{t}_g$ direction:

$$\underline{q}_{gc} \;=\; \underline{m}_{gc} + \bar{x}_c\underline{s}_g + \bar{y}_c\underline{t}_g \tag{29}$$

2.4 Final panel corner coordinates and diagonals

As a final step, we refer the temporary local corner coordinates $\bar{\underline{q}}_k$ to the updated origin and obtain the panel corners in local coordinates with respect to the centroid $\underline{q}_{gc}$.

$$\underline{q}_k \;=\; \bar{\underline{q}}_k - \begin{pmatrix} \bar{x}_c \\ \bar{y}_c \end{pmatrix} \tag{30}$$

The length of the panel diagonals are sometimes used to check on the geometry of panels:

$$g_1 = |\underline{q}_3 - \underline{q}_1| \qquad g_2 = |\underline{q}_4 - \underline{q}_2| \tag{31}$$

The longer diagonal $g_{\max} = \max(g_1, g_2)$ is often employed when approximation of the panel influence by point sources and dipoles are initiated.

3 Vector transformations

During the evaluation of the influences of a source/dipole panel onto a field point position vectors have to be transformed from the global coordinate system into the local coordinate system of the panel. Gradients of the potential (velocities) and Hessian matrices computed in the local coordinate system have to be transformed back into the global coordinate system.

A position vector $\underline{x}_g$ is converted from the global into a local coordinate system by the following transformation:

$$\underline{x} = \underline{\underline{T}}^T (\underline{x}_g - \underline{q}_{gc}) \quad \text{from global to local panel coordinate system} \tag{32}$$

A free vector like the velocity which does not require an origin as part of its definition is transformed via

$$\underline{v} = \underline{\underline{T}}^T \underline{v}_g \quad \text{from global to local panel coordinate system} \tag{33}$$

The back transformation is very simple. Because the coordinate system vectors are perpendicular to each other, dot products between them all vanish, i.e. $\underline{s}_g^T \underline{t}_g = 0$, $\underline{t}_g^T \underline{n}_g = 0$, and $\underline{n}_g^T \underline{s}_g = 0$. As a consequence, the inverse matrix $\underline{\underline{T}}^{-1}$ of matrix $\underline{\underline{T}}$ is equal to its transposed matrix $\underline{\underline{T}}^T$

$$\underline{\underline{T}}^{-1} \underline{\underline{T}} = \underline{\underline{T}}^T \underline{\underline{T}} = \underline{\underline{I}} = \begin{bmatrix} 1 & 0 & 0 \\ 0 & 1 & 0 \\ 0 & 0 & 1 \end{bmatrix} \tag{34}$$

Therefore, the back transformation is accomplished with either

$$\underline{v}_g = \underline{\underline{T}} \underline{v} \quad \text{velocity, from local panel to body-fixed coordinate system} \tag{35}$$

for velocities, or

$$\underline{x}_g = \underline{\underline{T}} \underline{x} + \underline{q}_{gc} \quad \text{position, from local panel to body-fixed coordinate system} \tag{36}$$

for position vectors.

For the back transformation of the matrix of local second order derivatives $\underline{\underline{H}}$ (Hessian) we use

$$\underline{\underline{H}}_g = \left(\underline{\underline{T}} \underline{\underline{H}} \right) \underline{\underline{T}}^T \tag{37}$$

In Fortran 95 these computations may be executed with the efficient `dot_multiply` and `matmul` functions. In Python similar functionality is provided by the `Numpy` package.

4 Constant Source Panel

In this section we summarize the equations needed to evaluate the influence of a panel with a distribution of sources onto a field point $\underline{p}$. In most procedures the collocation point will be the center of another or the same panel.

Again, all summations below make use of the cyclic definition of the index k, which takes values from 1 through 4 representing the number of a panel edge or corner. In case $k = 4$ the value of $k + 1 = 5$ is set to

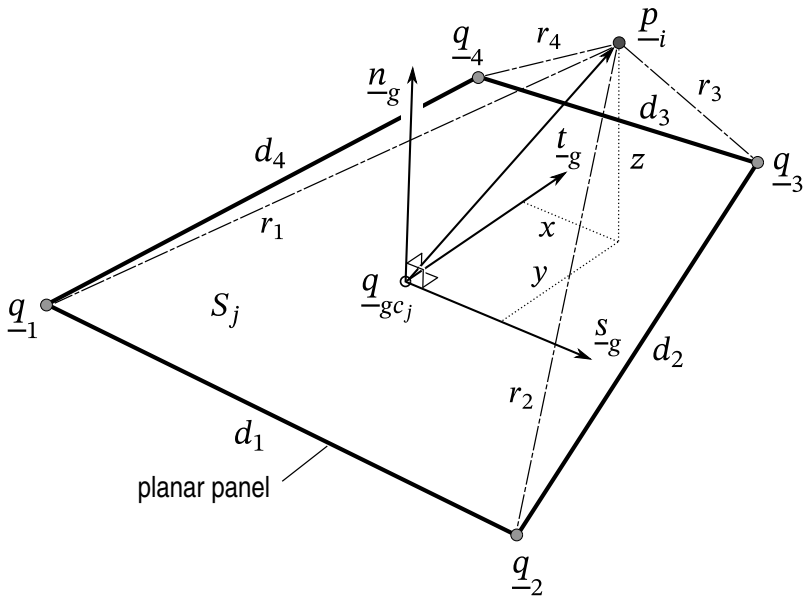

Figure 4: Field point $\underline{p}_i$ in the local coordinate system and quantities used in the evaluation of potential and derivatives

$k+1 := 1$. All coordinates are with respect to the coordinate system local to the planar quadrilateral panel (Figure 4).

The formulas for potential, gradient and Hessian matrix below make use of the following definitions and auxiliary terms already introduced by Hess and Smith (Hess and Smith, 1962):

$(x, y, z)^T$ local coordinates of field point $\underline{p}_i$ where we evaluate potential and derivatives

$(x_k, y_k)^T$ local coordinates of panel corners $\underline{q}_k$ with $k = 1, 2, 3, 4$; $z_k = 0$ in panel plane

$$d_k = \sqrt{(x_{k+1} - x_k)^2 + (y_{k+1} - y_k)^2} \qquad \text{length of panel edge } k \tag{38}$$

$$e_k = (x - x_k)^2 + z^2 \tag{39}$$

$$h_k = (x - x_k)(y - y_k) \tag{40}$$

$$m_k = \frac{(y_{k+1} - y_k)}{(x_{k+1} - x_k)} \qquad \text{tangens of angle between } x\text{−axis and edge } k \tag{41}$$

$$r_k = \sqrt{(x - x_k)^2 + (y - y_k)^2 + z^2} \qquad \text{distance from panel corner } \underline{q}_k \text{ to field point } \underline{p}_i \tag{42}$$

For some of the second order derivatives we also use the following abbreviations to shorten the presented equations.

$$\varrho_k = \left[r_k\, r_{k+1} + (x - x_k)(x - x_{k+1}) + (y - y_k)(y - y_{k+1}) + z^2\right] \tag{43}$$

$$\lambda_k = \left[(x - x_k)(y - y_{k+1}) - (x - x_{k+1})(y - y_k)\right] \tag{44}$$

4.1 Velocity potential for a constant source distribution

The contribution to the overall potential by a panel with constant source strength is

$$\phi_j = \sigma_j\, \phi \tag{45}$$

The potential induced by a panel with unit source strength is

$$\phi = \frac{-1}{4\pi}\sum_{k=1}^{4}\left\{\left[\frac{(x-x_k)(y_{k+1}-y_k)-(y-y_k)(x_{k+1}-x_k)}{d_k}\right]\ln\left(\frac{r_k+r_{k+1}-d_k}{r_k+r_{k+1}+d_k}\right)\right.$$
$$\left. + z\left[\tan^{-1}\left(\frac{m_k\, e_k - h_k}{z\, r_k}\right) - \tan^{-1}\left(\frac{m_k\, e_{k+1} - h_{k+1}}{z\, r_{k+1}}\right)\right]\right\} \quad (46)$$

An element of the sum in Equation (46) represents the contribution by panel edge k. Computation of an element is skipped if the edge is of zero length $d_k = 0$.

The last term in Equation (46) looks slightly different from the formula given by Katz and Plotkin (Katz and Plotkin, 2001). The formulation here implies that the standard inverse tangent function `atan()` or `arctan()` is used rather than its alternative `atan2()` or `arctan2()` provided in Fortran and Python, respectively.

4.2 Velocities induced by a constant source distribution

The components of a velocity vector $\underline{v}$ in local coordinates follow from the spatial derivatives of Equation (46):

$$\phi_x = \frac{\partial\phi}{\partial x} = \frac{-1}{4\pi}\sum_{k=1}^{4}\frac{y_{k+1}-y_k}{d_k}\ln\left(\frac{r_k+r_{k+1}-d_k}{r_k+r_{k+1}+d_k}\right) \quad (47)$$

$$\phi_y = \frac{\partial\phi}{\partial y} = \frac{-1}{4\pi}\sum_{k=1}^{4}\frac{-(x_{k+1}-x_k)}{d_k}\ln\left(\frac{r_k+r_{k+1}-d_k}{r_k+r_{k+1}+d_k}\right) \quad (48)$$

$$\phi_z = \frac{\partial\phi}{\partial z} = \frac{-1}{4\pi}\sum_{k=1}^{4}\left[\tan^{-1}\left(\frac{m_k\, e_k - h_k}{z\, r_k}\right) - \tan^{-1}\left(\frac{m_k\, e_{k+1} - h_{k+1}}{z\, r_{k+1}}\right)\right] \quad (49)$$

Again, only edges of nonzero length $d_k > 0$ contribute to the sum.

The velocity $\underline{v}_{ij} = \sigma_j(\phi_x, \phi_y, \phi_z)^T$ induced at point $\underline{p}_i$ by panel S_j is computed in local coordinates. The result is transformed back into the global coordinate system via Equation (35). A dot product with the normal vector $\underline{n}_{g_i}$ yields the velocity in direction of the surface normal at point $\underline{p}_i$.

4.3 Second order derivatives of a constant source distribution

Rather than using numerical differentiation of the velocity it may be preferable to compute the second order derivatives of the potential directly. For instance, Janson compares the use of numerical forward differencing with the direct computation of the second order derivatives in the evaluation of the free surface boundary condition of wave resistance problems (Janson, 1997).

Formulas are given below for a total of nine second order derivatives in the Hessian matrix. However, only six are truly needed due to the symmetry of Hessian matrices. Implementation of the remaining three may prove useful during the testing phase of the library. The back transformation (37) requires that all six local second order derivatives be computed, regardless whether just one, a select few, or all of the second order derivatives are needed in the global coordinate system.

$$\phi_{xx} = \frac{\partial^2\phi}{\partial x^2} = \frac{-1}{4\pi}\sum_{k=1}^{4}\frac{2(y_{k+1}-y_k)}{\left((r_k+r_{k+1})^2-d_k^2\right)}\left[\frac{(x-x_k)}{r_k}+\frac{(x-x_{k+1})}{r_{k+1}}\right] \quad (50)$$

$$\phi_{yx} = \frac{\partial^2\phi}{\partial y\partial x} = \frac{-1}{4\pi}\sum_{k=1}^{4}\frac{-2(x_{k+1}-x_k)}{\left((r_k+r_{k+1})^2-d_k^2\right)}\left[\frac{(x-x_k)}{r_k}+\frac{(x-x_{k+1})}{r_{k+1}}\right] \quad (51)$$

$$\phi_{zx} = \frac{\partial^2\phi}{\partial z\partial x} = \frac{-1}{4\pi}\sum_{k=1}^{4}\frac{z(y_{k+1}-y_k)(r_k+r_{k+1})}{(r_k\, r_{k+1})\,\varrho_k} \quad (52)$$

$$\phi_{xy} = \frac{\partial^2\phi}{\partial x\partial y} = \frac{-1}{4\pi}\sum_{k=1}^{4}\frac{2(y_{k+1}-y_k)}{\left((r_k+r_{k+1})^2-d_k^2\right)}\left[\frac{(y-y_k)}{r_k}+\frac{(y-y_{k+1})}{r_{k+1}}\right] \quad \text{equal to (51)} \tag{53}$$

$$\phi_{yy} = \frac{\partial^2\phi}{\partial y^2} = \frac{-1}{4\pi}\sum_{k=1}^{4}\frac{-2(x_{k+1}-x_k)}{\left((r_k+r_{k+1})^2-d_k^2\right)}\left[\frac{(y-y_k)}{r_k}+\frac{(y-y_{k+1})}{r_{k+1}}\right] \tag{54}$$

$$\phi_{zy} = \frac{\partial^2\phi}{\partial z\partial y} = \frac{-1}{4\pi}\sum_{k=1}^{4}\frac{-z(x_{k+1}-x_k)(r_k+r_{k+1})}{(r_k\,r_{k+1})\,\varrho_k} \tag{55}$$

$$\phi_{xz} = \frac{\partial^2\phi}{\partial x\partial z} = \frac{-1}{4\pi}\sum_{k=1}^{4}\frac{2(y_{k+1}-y_k)}{\left((r_k+r_{k+1})^2-d_k^2\right)}\left[\frac{z}{r_k}+\frac{z}{r_{k+1}}\right] \quad \text{equal to (52)} \tag{56}$$

$$\phi_{yz} = \frac{\partial^2\phi}{\partial y\partial z} = \frac{-1}{4\pi}\sum_{k=1}^{4}\frac{-2(x_{k+1}-x_k)}{\left((r_k+r_{k+1})^2-d_k^2\right)}\left[\frac{z}{r_k}+\frac{z}{r_{k+1}}\right] \quad \text{equal to (55)} \tag{57}$$

$$\phi_{zz} = \frac{\partial^2\phi}{\partial z^2} = \frac{-1}{4\pi}\sum_{k=1}^{4}\frac{\lambda_k\,(r_k+r_{k+1})}{(r_k\,r_{k+1})\,\varrho_k} \tag{58}$$

Obviously, the derivatives (50) through (58) still have to be multiplied by the source strength σ_j.

5 Constant Normal Dipole Panel

Source only panels are sufficient for displacement flows and among other application are extensively used in wave resistance computations and the flow around aircraft fuselages (Raven, 1996; Janson, 1997; Katz and Plotkin, 2001). Whenever lifting flows are considered, satisfying the Kutta condition at the trailing edge requires the use of vortex or dipole distributions. In fact, the effect of a constant normal dipole distribution is equivalent to a closed line vortex over the edges of the panel (Katz and Plotkin, 2001).

5.1 Velocity potential for a constant dipole distribution

The velocity potential ψ for a dipole distribution of constant unit strength with axis in the direction of the panel normal is equal to the negative of the normal velocity induced by a constant unit strength distribution of sources.

$$\psi = -\frac{\partial\phi}{\partial z} \qquad \text{see Equation (49)} \tag{59}$$

5.2 Velocities induced by a constant dipole distribution

The velocity components induced by a constant normal dipole distribution over panel S_j will be

$$\frac{\partial\psi}{\partial x} = -\frac{\partial^2\phi}{\partial z\partial x} \qquad \frac{\partial\psi}{\partial y} = -\frac{\partial^2\phi}{\partial z\partial y} \qquad \frac{\partial\psi}{\partial z} = -\frac{\partial^2\phi}{\partial z^2} \tag{60}$$

The required second order derivatives of the source potential are taken from Equations (52), (55) and (58). Of course, source strength σ_j is replaced by the dipole strength μ_j.

5.3 Second order derivatives of a constant dipole potential

For the implementation of nonlinear boundary conditions second order derivatives may be necessary. Again, equations for all nine second order derivatives are provided for testing purposes. Ultimately, only six are needed and symmetry of the Hessian may be enforced by copying the off-diagonal elements.

Formulas for the second order derivatives have been arranged to consist of common factors and to avoid divisions by zero during their computation.

$$\frac{\partial^2\psi}{\partial x^2} = \frac{-1}{4\pi}\sum_{k=1}^{4} z\,(y_{k+1}-y_k)\frac{(r_k+r_{k+1})}{\varrho_k\,(r_k r_{k+1})^2}\left\{(x-x_k)\left[\frac{r_k r_{k+1}(r_k+r_{k+1})^2+\varrho_k r_{k+1}^2}{\varrho_k r_k(r_k+r_{k+1})}\right]\right.$$
$$\left.+\,(x-x_{k+1})\left[\frac{r_k r_{k+1}(r_k+r_{k+1})^2+\varrho_k r_k^2}{\varrho_k r_{k+1}(r_k+r_{k+1})}\right]\right\} \quad (61)$$

$$\frac{\partial^2\psi}{\partial x\partial y} = \frac{-1}{4\pi}\sum_{k=1}^{4} z\,(y_{k+1}-y_k)\frac{(r_k+r_{k+1})}{\varrho_k\,(r_k r_{k+1})^2}\left\{(y-y_k)\left[\frac{r_k r_{k+1}(r_k+r_{k+1})^2+\varrho_k r_{k+1}^2}{\varrho_k r_k(r_k+r_{k+1})}\right]\right.$$
$$\left.+\,(y-y_{k+1})\left[\frac{r_k r_{k+1}(r_k+r_{k+1})^2+\varrho_k r_k^2}{\varrho_k r_{k+1}(r_k+r_{k+1})}\right]\right\} \quad (62)$$

$$\frac{\partial^2\psi}{\partial x\partial z} = \frac{-1}{4\pi}\sum_{k=1}^{4} -(y_{k+1}-y_k)\frac{(r_k+r_{k+1})}{\varrho_k\,(r_k r_{k+1})^2}\left\{r_k r_{k+1} - z^2\frac{(r_k+r_{k+1})^2}{\varrho_k} - z^2\left[\frac{r_k^2-r_k r_{k+1}+r_{k+1}^2}{r_k r_{k+1}}\right]\right\} \quad (63)$$

$$\frac{\partial^2\psi}{\partial y\partial x} = \frac{-1}{4\pi}\sum_{k=1}^{4} -z\,(x_{k+1}-x_k)\frac{(r_k+r_{k+1})}{\varrho_k\,(r_k r_{k+1})^2}\left\{(x-x_k)\left[\frac{r_k r_{k+1}(r_k+r_{k+1})^2+\varrho_k r_{k+1}^2}{\varrho_k r_k(r_k+r_{k+1})}\right]\right.$$
$$\left.+\,(x-x_{k+1})\left[\frac{r_k r_{k+1}(r_k+r_{k+1})^2+\varrho_k r_k^2}{\varrho_k r_{k+1}(r_k+r_{k+1})}\right]\right\} \quad (64)$$

$$\frac{\partial^2\psi}{\partial y^2} = \frac{-1}{4\pi}\sum_{k=1}^{4} -z\,(x_{k+1}-x_k)\frac{(r_k+r_{k+1})}{\varrho_k\,(r_k r_{k+1})^2}\left\{(y-y_k)\left[\frac{r_k r_{k+1}(r_k+r_{k+1})^2+\varrho_k r_{k+1}^2}{\varrho_k r_k(r_k+r_{k+1})}\right]\right.$$
$$\left.+\,(y-y_{k+1})\left[\frac{r_k r_{k+1}(r_k+r_{k+1})^2+\varrho_k r_k^2}{\varrho_k r_{k+1}(r_k+r_{k+1})}\right]\right\} \quad (65)$$

$$\frac{\partial^2\psi}{\partial y\partial z} = \frac{-1}{4\pi}\sum_{k=1}^{4} (x_{k+1}-x_k)\frac{(r_k+r_{k+1})}{\varrho_k\,(r_k r_{k+1})^2}\left\{r_k r_{k+1} - z^2\frac{(r_k+r_{k+1})^2}{\varrho_k} - z^2\left[\frac{r_k^2-r_k r_{k+1}+r_{k+1}^2}{r_k r_{k+1}}\right]\right\} \quad (66)$$

$$\frac{\partial^2\psi}{\partial z\partial x} = \frac{-1}{4\pi}\sum_{k=1}^{4}\frac{(r_k+r_{k+1})}{\varrho_k\,(r_k r_{k+1})^2}\left\{(x-x_k)\,\lambda_k\left[\frac{r_k r_{k+1}(r_k+r_{k+1})^2+\varrho_k r_{k+1}^2}{\varrho_k r_k(r_k+r_{k+1})}\right]\right.$$
$$\left.+(x-x_{k+1})\,\lambda_k\left[\frac{r_k r_{k+1}(r_k+r_{k+1})^2+\varrho_k r_k^2}{\varrho_k r_{k+1}(r_k+r_{k+1})}\right]+(y_{k+1}-y_k)\,r_k r_{k+1}\right\} \quad (67)$$

$$\frac{\partial^2\psi}{\partial z\partial y} = \frac{-1}{4\pi}\sum_{k=1}^{4}\frac{(r_k+r_{k+1})}{\varrho_k\,(r_k r_{k+1})^2}\left\{(y-y_k)\,\lambda_k\left[\frac{r_k r_{k+1}(r_k+r_{k+1})^2+\varrho_k r_{k+1}^2}{\varrho_k r_k(r_k+r_{k+1})}\right]\right.$$
$$\left.+(y-y_{k+1})\,\lambda_k\left[\frac{r_k r_{k+1}(r_k+r_{k+1})^2+\varrho_k r_k^2}{\varrho_k r_{k+1}(r_k+r_{k+1})}\right]-(x_{k+1}-x_k)\,r_k r_{k+1}\right\} \quad (68)$$

$$\frac{\partial^2\psi}{\partial z^2} = \frac{-1}{4\pi}\sum_{k=1}^{4} z\,\frac{\lambda_k(r_k+r_{k+1})}{\varrho_k\,(r_k r_{k+1})^2}\left[\frac{(r_k+r_{k+1})^2}{\varrho_k}+\frac{r_k^2-r_k r_{k+1}+r_{k+1}^2}{r_k r_{k+1}}\right] \quad (69)$$

6 Approximation formulas

In cases where the field point $\underline{p}_i = (x, y, z)^T$ is far enough away from the panel, the influence of the constant source or dipole panel on the field point may be approximated by the effect of a point source or point dipole potential.

3D point source potential: $$\hat{\phi} = \frac{-\sigma}{4\pi r} \quad (70)$$

3D point dipole potential (axis in panel normal direction): $$\hat{\psi} = \frac{-\mu z}{4\pi r^3} \quad (71)$$

As before, the computations are performed in the coordinate system local to the panel.

Far enough depends on the accuracy requirements of the flow solver. For sources Hess and Smith (1964) used the following criteria: An approximation of the constant source distribution by a single point source is justified if the distance r between panel origin $\underline{q}_{gc_j}$ and field point $\underline{p}_i$ is at least four times the largest panel diagonal $g_{\max}$ (see Section 2.4).

$$r = |\underline{p}_i - \underline{q}_{gc}| = \sqrt{x^2+y^2+z^2} > 4\,g_{\max} \quad (72)$$

The equations for the derivatives of a point source and a point dipole are readily available through computer algebra systems.

7 Test Data

Data is provided for three test cases:

1. a flat square panel (Figure 5),
2. a quadrilateral panel with a slight twist (Figure 6), and
3. a triangular panel (Figure 7).

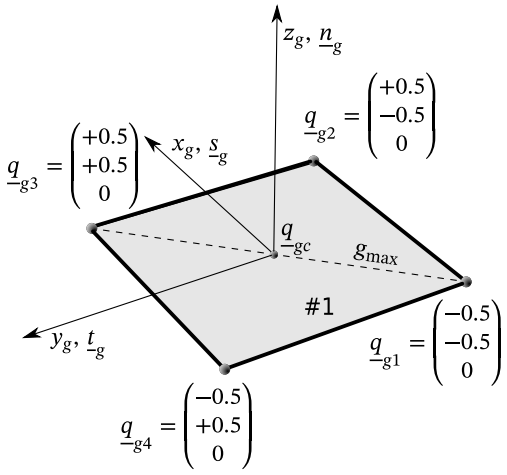

	center	transformation matrix		
	$\underline{q}_{gc}$	$\underline{s}_g$	$\underline{t}_g$	$\underline{n}_g$
x_g	0.00000000	1.00000000	0.00000000	0.00000000
y_g	0.00000000	0.00000000	1.00000000	0.00000000
z_g	0.00000000	0.00000000	0.00000000	1.00000000
	local corner coordinates ($z = 0$)			
	$\underline{q}_1$	$\underline{q}_2$	$\underline{q}_3$	$\underline{q}_4$
x	−0.50000000	0.50000000	0.50000000	−0.50000000
y	−0.50000000	−0.50000000	0.50000000	0.50000000

area	max. diagonal
A	$g_{\max}$
1.00000000	1.41421356

Figure 5: Geometry of test panel #1 (square)

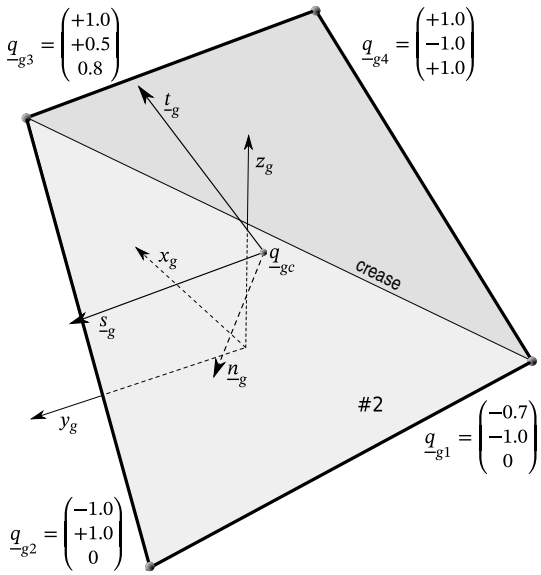

	center	transformation matrix		
	$\underline{q}_{gc}$	$\underline{s}_g$	$\underline{t}_g$	$\underline{n}_g$
x_g	0.03196586	−0.08526306	0.89595433	0.43588536
y_g	−0.10980295	0.99473574	0.10150419	−0.01406082
z_g	0.42891789	−0.05684204	0.43239188	−0.89989235
	local corner coordinates ($z = 0$)			
	$\underline{q}_1$	$\underline{q}_2$	$\underline{q}_3$	$\underline{q}_4$
x	−0.79872060	1.21632980	0.50296217	−1.00050985
y	−0.93162733	−0.99740524	1.08966483	1.02388691

area	max. diagonal
A	$g_{\max}$
3.55598088	3.00000000

Figure 6: Geometry of test panel #2 (twisted quadrilateral)

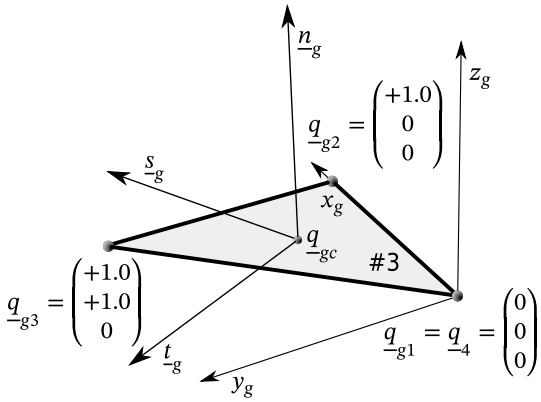

	center	transformation matrix		
	$\underline{q}_{gc}$	$\underline{s}_g$	$\underline{t}_g$	$\underline{n}_g$
x_g	0.66666667	0.89442719	−0.44721360	0.00000000
y_g	0.33333333	0.44721360	0.89442719	0.00000000
z_g	0.00000000	0.00000000	0.00000000	1.00000000
	local corner coordinates ($z = 0$)			
	$\underline{q}_1$	$\underline{q}_2$	$\underline{q}_3$	$\underline{q}_4$
x	−0.74535599	0.14907120	0.59628479	−0.74535599
y	−0.00000000	−0.44721360	0.44721360	−0.00000000

area	max. diagonal
A	$g_{\max}$
0.50000000	1.41421356

Figure 7: Geometry of test panel #3 (triangle)

Table 1: Results for unit strength source distribution on test panel No. #1 (square)

#		field point $\underline{p}_g$	field point $\underline{p}$ (local)	source potential ϕ	velocity $\underline{v}_{g_{ij}}$ (global)	Hessian matrix (global) $\phi_{xx}, \phi_{yx}, \phi_{zx}$	$\phi_{xy}, \phi_{yy}, \phi_{zy}$	$\phi_{xz}, \phi_{yz}, \phi_{zz}$
1	$x_{[g]}$	0.000	0.00000000		0.00000000	0.00882663	0.00000000	0.00000000
	$y_{[g]}$	0.000	0.00000000	−0.03899412	0.00000000	0.00000000	0.00882663	0.00000000
	$z_{[g]}$	2.000	2.00000000		0.01873493	0.00000000	0.00000000	−0.01765326
2	$x_{[g]}$	0.000	0.00000000		0.00000000	0.18377630	0.00000000	0.00000000
	$y_{[g]}$	0.000	0.00000000	−0.12626703	0.00000000	0.00000000	0.18377630	0.00000000
	$z_{[g]}$	−0.500	−0.50000000		−0.16666667	0.00000000	0.00000000	−0.36755260
3	$x_{[g]}$	0.500	0.50000000		0.03064217	0.03062433	−0.07906868	0.00000000
	$y_{[g]}$	1.000	1.00000000	−0.07396339	0.06513339	−0.07906868	−0.11292475	0.00000000
	$z_{[g]}$	0.000	0.00000000		0.00000000	0.00000000	0.00000000	0.08230042
4	$x_{[g]}$	−0.250	−0.25000000		−0.04024089	0.14364770	0.02766957	0.10965628
	$y_{[g]}$	0.250	0.25000000	−0.11549639	0.04024089	0.02766957	0.14364770	−0.10965628
	$z_{[g]}$	0.500	0.50000000		0.13755683	0.10965628	−0.10965628	−0.28729541
5	$x_{[g]}$	0.100	0.10000000		0.00001536	0.00015354	−0.00000028	−0.00000572
	$y_{[g]}$	0.400	0.40000000	−0.00992118	0.00006145	−0.00000028	0.00015248	−0.00002286
	$z_{[g]}$	8.000	8.00000000		0.00123369	−0.00000572	−0.00002286	−0.00030602

Table 2: Test data for unit strength dipole distribution on panel No. #1 (square)

#		field point $\underline{p}_g$	field point $\underline{p}$ (local)	dipole potential ψ	velocity $\underline{v}_{g_{ij}}$ (global)	Hessian matrix (global) $\psi_{xx}, \psi_{yx}, \psi_{zx}$	$\psi_{xy}, \psi_{yy}, \psi_{zy}$	$\psi_{xz}, \psi_{yz}, \psi_{zz}$
1	$x_{[g]}$	0.000	0.00000000		0.00000000	0.01223036	0.00000000	0.00000000
	$y_{[g]}$	0.000	0.00000000	−0.01873493	0.00000000	0.00000000	0.01223036	0.00000000
	$z_{[g]}$	2.000	2.00000000		0.01765326	0.00000000	0.00000000	−0.02446073
2	$x_{[g]}$	0.000	0.00000000		0.00000000	−0.49007013	0.00000000	0.00000000
	$y_{[g]}$	0.000	0.00000000	0.16666667	0.00000000	0.00000000	−0.49007013	0.00000000
	$z_{[g]}$	−0.500	−0.50000000		0.36755260	0.00000000	0.00000000	0.98014026
3	$x_{[g]}$	0.500	0.50000000		0.00000000	0.00000000	0.00000000	0.11084673
	$y_{[g]}$	1.000	1.00000000	−0.00000000	0.00000000	0.00000000	0.00000000	0.26508651
	$z_{[g]}$	0.000	0.00000000		−0.08230042	0.11084673	0.26508651	0.00000000
4	$x_{[g]}$	−0.250	−0.25000000		−0.10965628	0.42061658	0.10071871	0.32781345
	$y_{[g]}$	0.250	0.25000000	−0.13755683	0.10965628	0.10071871	0.42061658	−0.32781345
	$z_{[g]}$	0.500	0.50000000		0.28729541	0.32781345	−0.32781345	−0.84123315
5	$x_{[g]}$	0.100	0.10000000		0.00000572	0.00005711	−0.00000018	−0.00000283
	$y_{[g]}$	0.400	0.40000000	−0.00123369	0.00002286	−0.00000018	0.00005646	−0.00001132
	$z_{[g]}$	8.000	8.00000000		0.00030602	−0.00000283	−0.00001132	−0.00011357

For the square panel #1 global and local coordinate systems coincide so that it can be used to test the local formulas without potential errors due to a faulty transformation. Input and geometric data are shown in Figure 5. Results of the computation with source and dipole distributions are presented in Tables 1 and 2. Numbers with eight decimals are provided for the local field point coordinates, potential, velocity and Hessian matrix of second order derivatives. The latter are stated in global coordinates. The five test points have been chosen to test for symmetry and critical cases. Note that an evaluation of the induced velocities and second order derivatives is not possible directly on the panel edges.

Test panel #2 is also a quadrilateral but it is asymmetric and it has a slight twist. Hence the local coordinates do not coincide exactly with the input points. As described in Section 2, they form a flat replacement panel. This test case requires proper implementation of the coordinate transformation. Its local coordinates of the

Table 3: Results for unit strength source distribution on test panel No. #2 (twisted quadrilateral)

#		field point $\underline{p}_g$	field point $\underline{p}$ (local)	source potential ϕ	velocity $\underline{v}_{g_{ij}}$ (global)	Hessian matrix (global) $\phi_{xx}, \phi_{yx}, \phi_{zx}$	$\phi_{xy}, \phi_{yy}, \phi_{zy}$	$\phi_{xz}, \phi_{yz}, \phi_{zz}$
1	$x_{[g]}$	0.000	0.02264691		−0.01212182	0.03946923	0.00396796	0.02181863
	$y_{[g]}$	0.000	0.66182865	−0.16522813	0.00696597	0.00396796	0.04495038	−0.00996329
	$z_{[g]}$	2.000	−1.42928215		0.08803249	0.02181863	−0.00996329	−0.08441961
2	$x_{[g]}$	1.000	−0.98982354		0.26364529	−0.12324138	1.20482974	0.69400251
	$y_{[g]}$	−1.000	0.94259724	−0.26489432	−0.27501439	1.20482974	0.06958128	−1.03881191
	$z_{[g]}$	0.812	0.08973614		−0.06608018	0.69400251	−1.03881191	0.05366010
3	$x_{[g]}$	2.000	−0.14930027		0.06825884	−0.05893860	−0.00315626	0.03409464
	$y_{[g]}$	−0.110	1.62102729	−0.14240410	0.00213854	−0.00315626	0.03356511	0.00225823
	$z_{[g]}$	0.100	1.15383073		−0.02095174	0.03409464	0.00225823	0.02537348
4	$x_{[g]}$	0.500	−0.39798420		0.10713328	0.03019263	0.04922130	0.15900323
	$y_{[g]}$	−0.500	0.15103078	−0.27506722	−0.05606261	0.04922130	0.14063479	−0.07148362
	$z_{[g]}$	−0.100	0.68546488		−0.17949664	0.15900323	−0.07148362	−0.17082742
5	$x_{[g]}$	1.500	0.02264691		0.00048221	0.00029514	0.00000698	0.00014903
	$y_{[g]}$	−0.500	−2.80130259	−0.02954344	−0.00012699	0.00000698	0.00031784	−0.00003903
	$z_{[g]}$	−9.000	9.13039218		−0.00303477	0.00014903	−0.00003903	−0.00061298

Table 4: Test data for unit strength dipole distribution on panel No. #2 (twisted quadrilateral)

#		field point $\underline{p}_g$	field point $\underline{p}$ (local)	dipole potential ψ	velocity $\underline{v}_{g_{ij}}$ (global)	Hessian matrix (global) $\psi_{xx}, \psi_{yx}, \psi_{zx}$	$\psi_{xy}, \psi_{yy}, \psi_{zy}$	$\psi_{xz}, \psi_{yz}, \psi_{zz}$
1	$x_{[g]}$	0.000	0.02264691		0.00248615	−0.05548064	−0.00700073	−0.02149945
	$y_{[g]}$	0.000	0.66182865	0.08460143	−0.01006343	−0.00700073	−0.06030659	0.01781290
	$z_{[g]}$	2.000	−1.42928215		−0.08561907	−0.02149945	0.01781290	0.11578723
2	$x_{[g]}$	1.000	−0.98982354		0.69518756	2.84979321	12.70081520	5.04639151
	$y_{[g]}$	−1.000	0.94259724	−0.17825110	−1.45900817	12.70081520	0.61467602	−16.33371698
	$z_{[g]}$	0.812	0.08973614		−0.26882377	5.04639151	−16.33371698	−3.46446922
3	$x_{[g]}$	2.000	−0.14930027		0.05632760	−0.08769162	−0.00743156	0.01324037
	$y_{[g]}$	−0.110	1.62102729	−0.04857727	0.00387989	−0.00743156	0.03386797	0.00305246
	$z_{[g]}$	0.100	1.15383073		0.00800380	0.01324037	0.00305246	0.05382366
4	$x_{[g]}$	0.500	−0.39798420		0.13061736	0.03627333	0.06885842	0.21614830
	$y_{[g]}$	−0.500	0.15103078	−0.20901377	−0.08380497	0.06885842	0.24543310	−0.09649790
	$z_{[g]}$	−0.100	0.68546488		−0.22403859	0.21614830	−0.09649790	−0.28170643
5	$x_{[g]}$	1.500	0.02264691		0.00000556	0.00009654	0.00000149	0.00001755
	$y_{[g]}$	−0.500	−2.80130259	−0.00294294	−0.00003370	0.00000149	0.00009431	−0.00001442
	$z_{[g]}$	−9.000	9.13039218		−0.00061712	0.00001755	−0.00001442	−0.00019085

field points serve as a test for the correctness of the transformation matrix $\underline{\underline{T}}$. Input and geometric data are shown in Figure 6. Tables 3 and 4 list results for five field points.

The final test case #3 is a triangular panel. First and last corner point coincide which is the preferred method to state input for triangular panels. Input and geometric data are shown in Figure 7. Tables 5 and 6 present the results for constant source and dipole distributions respectively. Again, field points have been selected to uncover common programming mistakes.

Table 5: Results for unit strength source distribution on test panel No. #3 (triangle)

#		field point $\underline{p}_g$	field point $\underline{p}$ (local)	source potential ϕ	velocity $\underline{v}_{g_{ij}}$ (global)	Hessian matrix (global) $\phi_{xx}, \phi_{yx}, \phi_{zx}$	$\phi_{xy}, \phi_{yy}, \phi_{zy}$	$\phi_{xz}, \phi_{yz}, \phi_{zz}$
1	$x_{[g]}$	0.000	−0.74535599		−0.00255504	0.00284679	−0.00054992	0.00324874
	$y_{[g]}$	0.000	−0.00000000	−0.01847387	−0.00124116	−0.00054992	0.00365068	0.00155038
	$z_{[g]}$	2.000	2.00000000		0.00801178	0.00324874	0.00155038	−0.00649747
2	$x_{[g]}$	0.000	−0.74535599		−0.03515188	−0.01061033	−0.03492704	−0.08488264
	$y_{[g]}$	0.000	−0.00000000	−0.04558955	−0.01569148	−0.03492704	0.05305165	−0.03624921
	$z_{[g]}$	−0.500	−0.50000000		−0.03689590	−0.08488264	−0.03624921	−0.04244132
3	$x_{[g]}$	0.500	0.14907120		−0.03703739	−0.00000000	0.14235251	0.00000000
	$y_{[g]}$	1.000	0.67082039	−0.05806854	0.07533101	0.14235251	−0.15915494	0.00000000
	$z_{[g]}$	0.000	0.00000000		0.00000000	0.00000000	0.00000000	0.15915494
4	$x_{[g]}$	−0.250	−0.85715939		−0.03156649	−0.03685236	0.00174655	0.05415752
	$y_{[g]}$	0.250	0.33541020	−0.03856218	0.00016099	0.00174655	0.03685721	−0.00459836
	$z_{[g]}$	0.500	0.50000000		0.02101846	0.05415752	−0.00459836	−0.00000485
5	$x_{[g]}$	0.100	−0.47702784		−0.00004349	0.00007559	0.00000004	0.00001617
	$y_{[g]}$	0.400	0.31304952	−0.00495674	0.00000518	0.00000004	0.00007671	−0.00000194
	$z_{[g]}$	8.000	8.00000000		0.00061541	0.00001617	−0.00000194	−0.00015230

Table 6: Test data for unit strength dipole distribution on panel No. #3 (triangle)

#		field point $\underline{p}_g$	field point $\underline{p}$ (local)	dipole potential ψ	velocity $\underline{v}_{g_{ij}}$ (global)	Hessian matrix (global) $\psi_{xx}, \psi_{yx}, \psi_{zx}$	$\psi_{xy}, \psi_{yy}, \psi_{zy}$	$\psi_{xz}, \psi_{yz}, \psi_{zz}$
1	$x_{[g]}$	0.000	−0.74535599		−0.00324874	0.00283118	−0.00112649	0.00530627
	$y_{[g]}$	0.000	−0.00000000	−0.00801178	−0.00155038	−0.00112649	0.00453262	0.00247825
	$z_{[g]}$	2.000	2.00000000		0.00649747	0.00530627	0.00247825	−0.00736380
2	$x_{[g]}$	0.000	−0.74535599		0.08488264	0.10987586	0.13657907	0.25653419
	$y_{[g]}$	0.000	−0.00000000	0.03689590	0.03624921	0.13657907	−0.15326032	0.10586092
	$z_{[g]}$	−0.500	−0.50000000		0.04244132	0.25653419	0.10586092	0.04338446
3	$x_{[g]}$	0.500	0.14907120		0.00000000	0.00000000	0.00000000	−0.46066239
	$y_{[g]}$	1.000	0.67082039	−0.00000000	0.00000000	0.00000000	0.00000000	0.67419116
	$z_{[g]}$	0.000	0.00000000		−0.15915494	−0.46066239	0.67419116	0.00000000
4	$x_{[g]}$	−0.250	−0.85715939		−0.05415752	−0.15168451	0.02247476	0.07835304
	$y_{[g]}$	0.250	0.33541020	−0.02101846	0.00459836	0.02247476	0.06579680	−0.02160475
	$z_{[g]}$	0.500	0.50000000		0.00000485	0.07835304	−0.02160475	0.08588771
5	$x_{[g]}$	0.100	−0.47702784		−0.00001617	0.00002782	0.00000002	0.00000800
	$y_{[g]}$	0.400	0.31304952	−0.00061541	0.00000194	0.00000002	0.00002852	−0.00000097
	$z_{[g]}$	8.000	8.00000000		0.00015230	0.00000800	−0.00000097	−0.00005634

The implementation of the presented formulas used to assess the test cases has been extensively tested. Numerous students have used the presented equations and successfully implemented their own panel codes.

8 Conclusions

Despite the advances in computational fluid mechanics, potential theory based methods still have a wide range of applications in the design of aircraft, ships and their propulsion systems. Computational effort is usually small to moderate so that the programs can be applied in design optimization even if the design cycle is quite short. The present paper presents in concise form the necessary equations to program the core of a panel method based on constant strength source and dipole panels. With the provided test cases the reader is enabled to implement and test the core before it is applied in the context of a numerical analysis program.

References

Bal, S. (2008). Prediction of wave pattern and wave resistance of surface piercing bodies by a boundary element method. *Numerical Methods in Fluids*, 56(3):305–329. https://doi.org/10.1002/fld.1527.

Birk, L. (2009). Application of constraint multi-objective optimization to the design of offshore structure hulls. *Journal of Offshore Mechanics and Arctic Engineering*, 131(1):11301–1–11301–9.

Birk, L. (2019). *Fundamentals of ship hydrodynamics: fluid mechanics, ship resistance and propulsion*. Wiley & Sons, Hoboken, NJ.

Dawson, C. (1977). A practical computer method for solving ship-wave problems. In *2nd Int. Conf. on Numerical Ship Hydrodynamics*, Berkeley, CA.

Gaggero, S. and Brizzolara, S. (2009). A panel method for trans-cavitating marine propellers. In *Proc. of the 7th International Symposium on Cavitation – CAV2009*, Ann Arbor, MI.

Grigoropoulos, G., Harries, S., Damala, D., Birk, L., and Heimann, J. (2003). Seakeeping assessment for high-speed monohulls – a comparative study. In *Proc. of 8th Int. Marine Design Conference (IMDC 2003)*, Athens, Greece. National Technical University of Athens.

Harries, S. (1998). *Parametric design and hydrodynamic optimization of ship hull forms*. PhD thesis, Technische Universität Berlin (D83), Berlin.

Hess, J. (1972). Calculation of potential flow about arbitrary three-dimensional lifting bodies. Report No. MDC J5679-01, Douglas Aircraft Co., McDonnell Douglas Corporation, Long Beach, CA.

Hess, J. and Smith, A. (1962). Calculation of non-lifting potential flow about arbitrary three-dimensional bodies. Report No. E.S. 40622, Douglas Aircraft Co., Inc., Long Beach, CA.

Hess, J. and Smith, A. (1964). Calculation of non-lifting potential flow about arbitrary three-dimensional bodies. *Journal of Ship Research*, 8(2):22–44.

Hess, J. and Smith, A. (1967). Calculation of potential flow about arbitrary bodies. *Progress in Aeronautical Sciences*, 8:1–138.

Hsin, C.-Y., Kerwin, J., and Kinnas, S. (1991). A panel method for the analysis of the flow around highly skewd propellers. In *SNAME Propellers/Shafting '91 Symposium*, Virginia Beach, VA.

Janson, C.-E. (1997). *Potential flow panel methods for the calculation of free surface flows with lift*. PhD thesis, Department of Naval Architecture and Ocean Engineering, Chalmers University of Technology, Gothenburg, Sweden.

Jensen, G. (1988). Berechung der stationären Potentialströmung um ein Schiff unter Berücksichtigung der nichtlinearen Randbedingung an der Wasseroberfläche. Technical Report 484, Technische Universität Hamburg-Harburg.

J.L. H. and W.O., V. (1988). *Panel Methods in Fluid Mechanics with Emphasis on Aerodynamics*, volume 21 of *Notes on Numerical Fluid Mechanics*, chapter Application of an advanced panel method to aerodynamic problems of aircraft design, pages 79–90. Vieweg+Teubner Verlag, Wiesbaden. https://doi.org/10.1007/978-3-663-13997-3_6.

Katz, J. and Plotkin, A. (2001). *Low-speed aerodynamics*. Cambridge Aerospace Series. Cambridge University Press, New York, NY, second edition.

Kellogg, O. (1929). *Foundations of potential theory*. Springer, Berlin, Germany.

Kim, B. and Shin, Y. (2003). A NURBS panel method for three-dimensional radiation and diffraction problems. *Journal of Ship Research*, 47(2):177–186.

Kinnas, S., Fan, H., and Tian, Y. (2015). A panel method with a full wake alignment model for the prediction of the performance of ducted propellers. *Journal of Ship Research*, 59(4):246–257. `http://dx.doi.org/10.5957/JOSR.59.4.150057`.

Lee, C., Maniar, H., Newman, J., and Zhu, X. (1996). Computations of wave loads using a B-spline panel method. In *21st Symp. on Naval Hydrodynamics*, pages 44–59, Trondheim, Norway.

Maniar, H. (1995). *A three dimensional higher order panel method based on B-splines*. PhD thesis, Department of Ocean Engineering, Massachusetts Institute of Technology, Cambridge, MA, USA.

Mishima, S. and Kinnas, S. (1997). Application of a numerical optimization technique to the design of cavitating propellers in nonuniform flow. *Journal of Ship Research*, 41(2):93–107.

Nakos, D. (1990). *Ship wave patterns and motions by a three-dimensional Rankine panel method*. PhD thesis, Massachusetts Institute of Technology, Cambridge, MA, USA.

Newman, J. (1986). Distributions of sources and dipoles over a quadrilateral panel. *Journal of Engineering Mathematics*, 20:113–126.

Newman, J. and Sclavounos, P. (1988). The computation of wave loads on large offshore structures. In *Proc. of Int. Conf. on Behaviour of Offshore Structures (BOSS '88)*, pages 605–622, Trondheim, Norway.

Raven, H. (1996). *A solution method for the nonlinear ship wave resistance problem*. PhD thesis, Technical University Delft, Delft, The Netherlands.

Webster, W. (1975). The flow about arbitrary, three-dimensional smooth bodies. *Journal of Ship Research*, 19(4):206–218.

Yeung, R. (1973). A singularity-distribution method for free-surface flow problems with an oscillating body. Technical Report NA 73-6, College of Engineering, University of California Berkeley.